Noise generation of fluttering flag in a free stream

Article *in* Journal of Fluid Science and Technology · January 2021

DOI: 10.1299/jfst.2021jfst0005

4 authors, including:

Yasufumi Konishi
Tohoku University
42 PUBLICATIONS **153** CITATIONS

SEE PROFILE

Bulletin of the JSME Vol.16, No.1, 2021
Journal of Fluid Science and Technology

Noise generation of fluttering flag in a free stream

Reon NISHIKAWA*, Osamu TERASHIMA*, Yasufumi KONISHI** and Miyu OKUNO*
*Faculty of Engineering / Department of Mechanical Systems Engineering, Toyama Prefectural University
5180, Kurokawa, Imizu, Toyama 939-0398, Japan
E-mail: u053011@st.pu-toyama.ac.jp
**Institute of Fluid Science, Tohoku University
2-1-1, Katahira, Aoba-ku, Sendai, Miyagi 980-8577, Japan

Received: 29 February 2020; Revised: 18 October 2020; Accepted: 4 December 2020

Abstract
An experimental study on the noise from a fluttering flag was performed in a low-noise wind tunnel. In the experiment, simultaneous measurements of noise from the flag and its motion were performed using microphones and a camera, respectively, to obtain the noise characteristics and their relation. Additionally, simultaneous measurements of noise and its displacement were performed to quantitively discuss their relation using seven laser displacement sensors. The experimental results indicated that a highly periodic noise with significant directivity in the vertical direction is generated from the flag, and the dominant frequency of the noise is linearly proportional to the inlet velocity. Additionally, the constants of proportionality are inversely proportional to the length of the flag and the square root of its thickness. The results also indicated that the downstream edge of the flag rolls up and down when significant periodic sound pressure is generated by the flow near the downstream edge of the flag. Furthermore, near the center of the downstream edge, the flag flutters at the dominant frequency of the emitted noise with high two-dimensionality. Therefore, the fluttering region was observed as the source of significant periodic noise from the flag. It is also found that the vibration of the downstream edge which brought the noise generation was caused by the strong upward or downward flow which occurs periodically.

Keywords : Flag, Noise, Wind tunnel, Visualization, Displacement measurement, Particle image velocimetry

1. Introduction

Fluttering flag in flow has been investigated for a long time from both a physical and an engineering point of view. Pioneering work on fluttering flag was performed by Fairthorne (1930) and Thoma (1939). Fairthorne measured the drag coefficients of several types of flags in a wind tunnel and found the relationship between the length of the flag and its coefficient. Subsequently, significant work has been conducted to investigate the forces acting on fluttering flags (Emmanuel et al., 2013). Hoerner (1965) and Taneda (1968) investigated the relationship between the drag of a flag and its length, and obtained different relationships from those of Fairthorne. Furthermore, Taneda (1968) found that the frequency of the oscillation of the flag depended on the Reynolds number and the mass ratio of the flag. The traveling waves on a fluttering flag were found and discussed by Sparenberg (1962). These groundbreaking works led to later research on parachutes (Lokerson, 1968), vehicles (Bourrières, 1969), projectiles (Fancett and Calyden, 1972), and rockets (Auman and Wilks, 2005).

The fluttering flag remains a subject of interest for researchers. The time-averaged drag coefficients of fluttering flag were investigated and discussed in previous works (e.g., Wilk and Skuta, 2009), and a simple model was presented by Moretti (2003), which was later validated by Ristroph and Zhang (2008). More recently, the unsteady fluid force acting on a fluttering flag was measured, and the drag force and the moment around its strut were discussed from the perspective of its evolution during fluttering mode switches (Emmanuel et al., 2013). In addition, for the improvement of heat transfer, the flow-induced vibration of an inverted flag (Kim et al., 2013) has been studied by numerous researchers (Yu et al., 2017, Ryu et al., 2015, and Chen et al., 2018).

Paper No.20-00112
[DOI: 10.1299/jfst.2021jfst0005]

From the above discussion, it can be inferred that a flag in flow has been studied from a physical and engineering point of view. However, noise generation from a fluttering flag has not been explored in detail. This is because of the difficulties associated with simulating the noise from a fluttering flag with large amplitude in a flow. Hence, in this study, we performed experiments in a wind tunnel to investigate the characteristics and generation mechanism of the noise from the flag. First, the noise and motion of the flag were measured simultaneously in a low-noise wind tunnel to determine the characteristics of the emitted noise from the flag and the relation between the noise and its motion. Then, the noise and displacement of the flag were measured simultaneously in the low-noise wind tunnel to determine the relation quantitatively. Measurements of the displacement of the flag were performed using laser displacement sensors. Additionally, we performed velocity measurements near the downstream edge of the flag to investigate the relation between the motion of the flag and the velocity field.

2. Experimental

The experiments were performed in a suction-type low-noise wind tunnel at the Institute of Fluid Science, Tohoku University. The test section was an open-type configuration surrounded by an anechoic chamber. The shape of the nozzle exit was rectangular. The width and vertical length were 300 mm and 500 mm, respectively. The streamwise length of the test section (i.e., length between the nozzle exit and edge of the collector nozzle at the downstream side) was 1000 mm. The background noise level in the test section was less than 65 dB [A], where [A] denotes the A-weighted sound pressure level when the streamwise velocity of the free stream was 45 m/s.

Figure 1 shows the flag used in this study. It is made of polyester and the streamwise length l, width w, and thickness t are 410 mm, 300 mm, and 0.4 mm, respectively. The support bar of the flag was made of aluminum with a diameter of 8 mm. The weight of the flag without the bar m was 0.011 kg. The mass ratio (Taneda, 1968) MR is expressed in Eq. (1) and is approximately 0.18. Specifically, ρ denotes the density of the fluid.

$$\mathrm{MR} = \left(\frac{m}{l^2 \cdot w}\right) / \rho \tag{1}$$

Figure 2 shows a perspective view of the test section for simultaneous measurement of the noise from the flag and its motion. The coordinate system is defined as follows: the axial (streamwise) coordinate is x, the vertical (cross-streamwise) coordinate is y, the spanwise coordinate is z, and the origin is set at the center of the nozzle exit, as shown in Fig. 2. The flag was set at the exit of the nozzle ($y = 0$). Microphones (PCB Inc., 130F20) with a data logger (Keyence Inc., NR-500 and NR-CA04) to measure the noise were located at the bottom (x = 205 mm, y = -1000 mm, and z = 0, microphone 1) and side of the test section (x = 205 mm, y = 0, and z = 1,000 mm, microphone 2). A camera (Photron Inc., FASTCAM SA-X2) was set to obtain photographs of the flag in flow from the top and side view positions. The sampling frequency for noise measurement was 100 kHz. The frame rate, focal length, and aperture value of the lens (Nikon Inc., NIKKOR 35 mm F1.4) were 5000 fps, 35 mm, and f 1.4, respectively.

Figure 3 shows a perspective view of the test section for the simultaneous measurement of noise and displacement of the flag. The coordinate system is identical to that shown in Fig. 2. Microphone 1 was used to measure the noise. A laser displacement sensor (Keyence Inc., IL-300) connected to the signal amplifier (Keyence Inc., IL-1000) was used to measure the displacement of the flag. Seven sensors were set at the upper side of the flag (y = 300 mm), and spanwise profiles of the displacement were measured for several streamwise locations. The measurement positions of displacement along the spanwise direction were z = -105 mm, -70 mm, -35 mm, 0, 35 mm, 70 mm, and 105 mm. The reference distance, measurement range, spot diameter of the laser, accuracy of the linearity of the output signal, and accuracy of the repeatability were 300 mm, 160 to 450 mm, 0.5 mm, less than ±0.25%, and 30 μm, respectively. The output voltages of the amplifiers were obtained using a data-logger (Keyence Inc., NR-500 and NR-HA08). The sampling frequency for the displacement measurement was 3 kHz. The output voltage corresponded to 2.5 V when the displacement was 0 (i.e., the flag was the position at y = 0) and it corresponded to 5.0 V when the displacement was -150 mm (i.e., the flag was the position at y = -150 mm). Furthermore, the minimum measurement resolution of the output voltage was 1 mV. Hence, the minimum measurement resolution of the displacement by the present system estimated from the static calibration tests corresponds to 0.06 mm.

[DOI: 10.1299/jfst.2021jfst0005]

3. Results

3.1 Characteristics of generated noise

Figure 4 shows the results of frequency analysis of the sound pressure as measured by microphones 1 and 2 when the velocity at the nozzle exit U_∞ was 30 m/s. Specifically, U_∞ was measured using a Pitot tube that was connected to a micro manometer in which the sensing part was set at $x = z = 0$ and $y = 125$ mm. The sampling number and number of samples for averaging the measurement of the sound pressure were 100,000 and 10, respectively. The red and black line denote the noise from the flag measured by microphones 1 and 2, respectively. Similarly, the blue and green line show the background noise measured by microphones 1 and 2, respectively. The abscissa and ordinate correspond to the frequency and sound pressure level, respectively. The sound pressure level is calculated based on the minimum audible pressure, i.e., 2×10^{-5} Pa. Measured data using microphone 1 exhibit a distinct peak at 60 Hz. However, a small peak is detected in the corresponding data for microphone 2. Therefore, it is concluded that highly periodic sound pressure with a significant directivity in the vertical direction was generated from the fluttering flag.

Figure 5 shows the results of frequency analysis of the sound pressure measured by microphone 1 when the velocity at the nozzle exit U_∞ was 30 m/s and the width of the flag was 300 mm or 200 mm. In the present experiment, the width of the flag was almost the same as that of the nozzle exit. As shown in numerous previous studies, the width of the potential core region of the rectangular free jet becomes smaller towards the downstream side and it was approximately 190 mm in the present wind tunnel. Therefore, shear layers developing from the edge of the nozzle exit had an influence on the motion of the spanwise edge of the flag. However, as shown in Fig. 5, the dominant noise from the flag was not dependent on the width of the flag. When we used a flag with a width of 200 mm, the same dominant noise (60 Hz) was observed. However, noises higher or lower than 60 Hz became small. Therefore, we determined that the present flag allows the evaluation of the dominant noise from the flag.

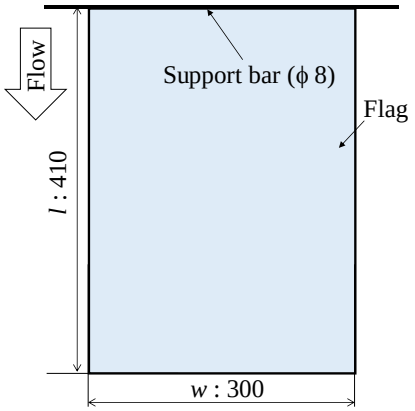

Fig. 1 Schematic view of the flag.

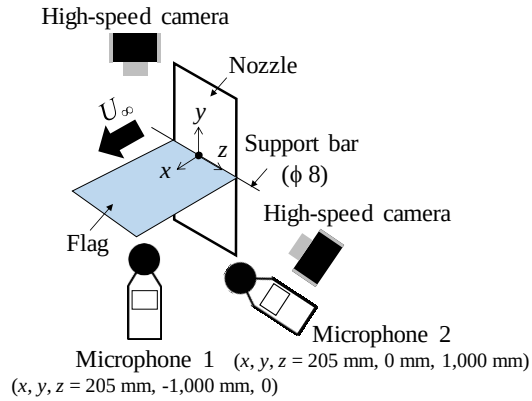

Fig. 2 Experimental setup for the simultaneous measurement of the noise and the motion of the flag.

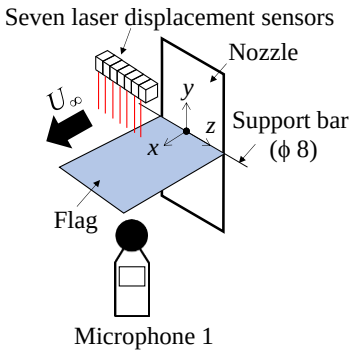

Fig. 3 Experimental setup for the simultaneous measurement of the noise and the displacement of the flag.

[DOI: 10.1299/jfst.2021jfst0005]

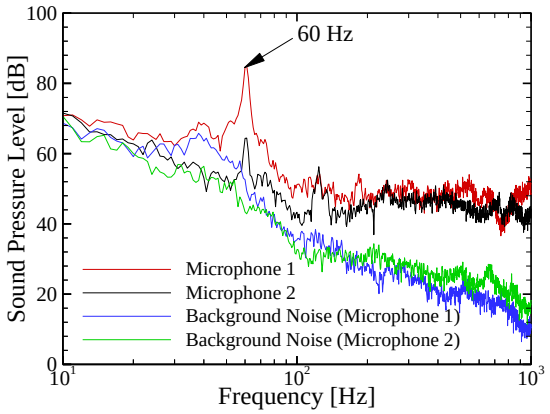

Fig. 4 Results of frequency analysis when U_∞ was 30 m/s.

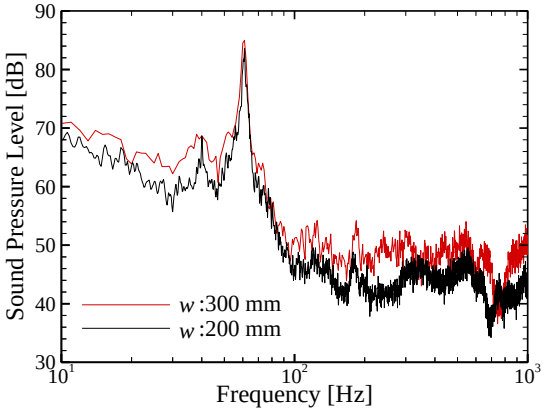

Fig. 5 Results of frequency analysis with two different flags (U_∞ = 30 m/s).

Hereafter, the main discussion will be on the noise measured via microphone 1.

Figure 6 shows the dependence of the relation between peak frequency f_p of the noise and U_∞ on l. The abscissa and ordinate correspond to U_∞ and f_p, respectively. Filled squares, triangles, and downward triangles correspond to the results of l = 410 mm, 288 mm, and 123 mm, respectively. The results indicate that f_p is linearly proportional to U_∞ and inversely proportional to l. Additionally, f_p is directly proportional to MR. The relationship obtained between f_p and U_∞ is shown in Eq. (2):

$$f_p = U_\infty / a\,(l) \tag{2}$$

Here, a (l) is a function of l. In the 3 cases shown in Fig. 6, a (l) corresponds to 0.50 (l = 410 mm), 0.44 (l = 287 mm), and 0.38 (l = 123 mm). We use the result to obtain a linear approximation equation that is expressed as Eq. (3). The square value of the correlation coefficient is 0.99. Eq. (3) shows that the natural frequency of the flag in a flow is inversely proportional to l, similarly to the vibration of the string when f_p is less than 91 Hz (i.e., in the condition of a (l) = 0.33 and l = 0). Therefore, it is considered to be the dominant noise from the flag, which is caused by vibration similar to that of a cantilever string.

$$a(l) = 0.42\,l + 0.33 \tag{3}$$

Figure 7 shows the dependence of the relationship between the peak frequency f_p of the noise and U_∞ on t. The abscissa and ordinate correspond to U_∞ and f_p, respectively. Filled squares, open triangles, and open downward triangles correspond to the results with t = 0.40 mm, 0.80 mm, and 1.20 mm, respectively. The results indicate that f_p is almost linearly proportional to U_∞ and inversely proportional to t (i.e., f_p is inversely proportional to MR). The relationship obtained between f_p and U_∞ using the non-dimensional frequency S_t and thickness l/t is shown in Eq. (4):

$$S_t = (l\,f_p)/U_\infty = A\sqrt{l/t} + B \tag{4}$$

Here, A and B are constants. In the present experimental conditions, A and B are approximately 0.04 and -0.40, respectively. These values are obtained from the linear approximation equation for the relation of S_t and $\sqrt{l/t}$ as shown in Fig. 8. The square value of the correlation coefficient is 0.99. Eq. (4) indicates that f_p is linearly proportional to $1/\sqrt{t}$, hence it is linearly proportional to $1/\sqrt{m}$ because the mass of the flag m depends on its thickness t. In general, the natural frequency of the vibrating object is linearly proportional to $1/\sqrt{m}$. Therefore, it is considered that the change in f_p in Fig. 7 was due to the change in the natural frequency of the flag.

Figure 9 shows the dependence of the relation between sound pressure level at f_p and U_∞ on t. The abscissa and ordinate correspond to U_∞ and sound pressure level at f_p, respectively. The meanings of symbols are identical to those in Fig. 7. Generally, with respect to the flow-induced noise from rigid bodies, the sound pressure level increases with an increase in the flow velocity (Blake 2017). However, for the fluttering flag, the relation significantly depends on the thickness of the flag. With respect to thick flags, the sound pressure level at f_p increases with increases in U_∞. However, for a thin flag, the sound pressure level when U_∞ is 25 m/s is higher than when U_∞ is 30 m/s. Additionally, for thick flags,

[DOI: 10.1299/jfst.2021jfst0005]

the increase rate of the sound pressure level is different. These results indicate that the generation mechanism of noise from the flag is different from that of the flow-induced noise from a rigid body. Further, Figs. 7 and 9 show that the sound pressure level depends on both f_p and U_∞. Therefore, it is considered that the sound pressure level depends on the natural frequency of the flag and the velocity field around the flag.

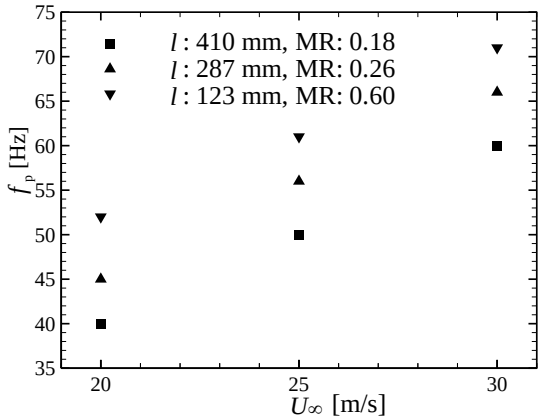

Fig. 6 Dependence of the relation between f_p and U_∞ on l.

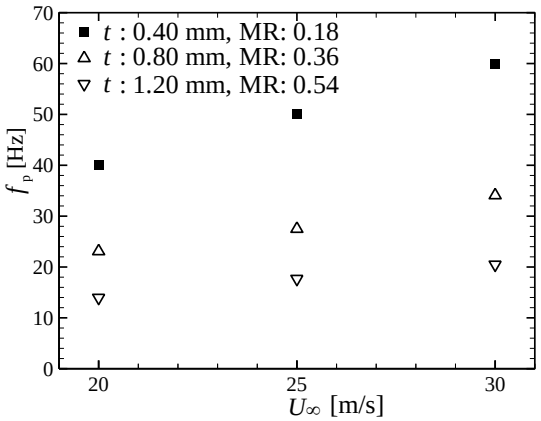

Fig. 7 Dependence of the relation between f_p and U_∞ on t.

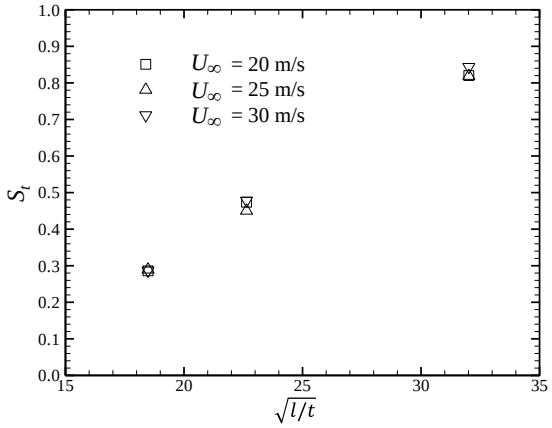

Fig. 8 Relations between $\sqrt{l/t}$ and S_t.

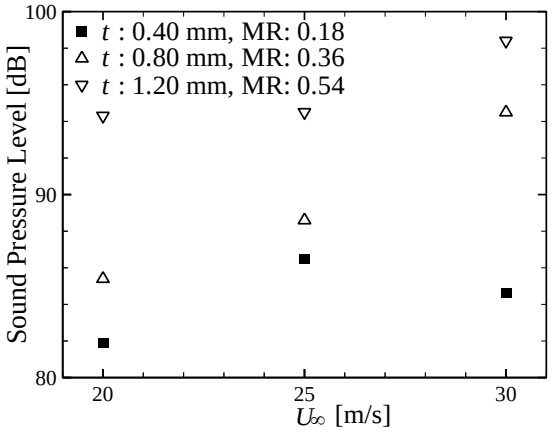

Fig. 9 Dependence of the relation between sound pressure level at f_p and U_∞ on t.

3.2 Motion of the flag

For the flag shown in Fig. 1, simultaneous measurement of the sound pressure and motion of the flag was performed.

Figures 10 and 11 show the motion of the flag. Figures 10 and 11 show the side and top views, respectively. Time 1, 2, and 3 in Figs. 10 and 11 correspond to the time when the sound pressure with frequency f_p as measured by microphone 1 correspond to top (Time 1), 0 (Time 2), and bottom (Time 3), respectively, as shown in Fig. 12. The signal is obtained by applying a bandpass filter with a center frequency f_p to measure the sound pressure using microphone 1. To verify the measured data, compensation of the time delay caused by the noise propagation from the flag to the microphone was performed. It was about 3 ms in this study. This value was determined using a speaker set above microphone 1 (x = 205 mm, y = 0, and z = 0), and placing the reference microphone just near the speaker. We calculated the cross-correlation coefficient of two signals and found the value for the compensation which maximizes the cross-correlation coefficient.

The results indicate that the near center of the downstream edge of the flag rolls down at Time 1 and rolls up at Time 2 with two-dimensionality. The findings also reveal that the spanwise edge of the downstream side of the flag randomly flutters with three-dimensionality. Therefore, it is concluded that there is a possibility that the rolling up and down of the flag at the downstream edge is the main cause for the noise generation from the flag.

3.3 Displacement of the flag

In this section, the measured results of displacement D are discussed. It should be noted that the time variation in D is termed as displacement fluctuation. In this section, we focus on the flag whose length and thickness are 410 mm and

[DOI: 10.1299/jfst.2021jfst0005]

0.40 mm, respectively.

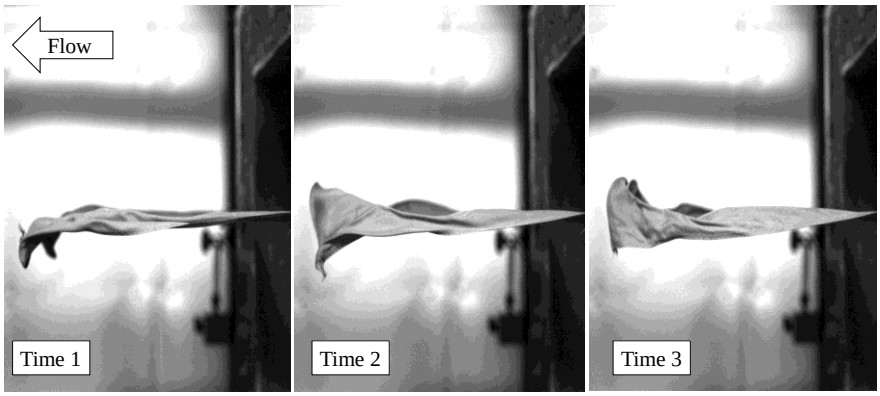

Fig. 10 Motions of the fluttering flag (Side view, U_∞ = 30 m/s).

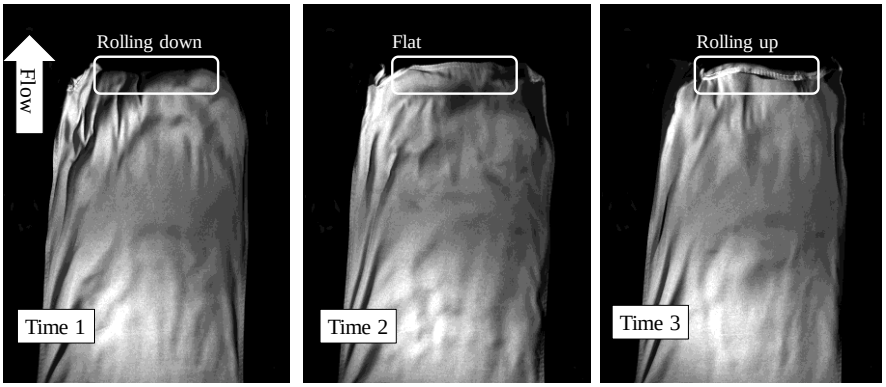

Fig. 11 Motions of the fluttering flag (Top view, U_∞ = 30 m/s).

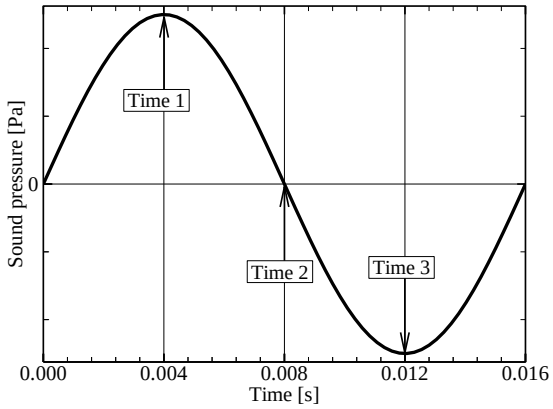

Fig. 12 Definition of Time 1, Time 2, and Time 3.

Figure 13 shows the streamwise profiles of root mean square (rms) value of displacement fluctuation D_{rms}. The abscissa and ordinate correspond to x and D_{rms}, respectively. Filled squares and triangles denote D_{rms} that is calculated by using all fluctuations of D and only the fluctuating component of f_p. The number of data points used for the calculation of D_{rms} is 30,000. The results indicate that D_{rms} increases near the downstream edge of the flag in both cases. However, there are differences in the streamwise position, where the value of D_{rms} is maximum. Specifically, D_{rms} calculated using all fluctuations is maximum at x = 380 mm and that calculated using only the fluctuation of f_p is maximum at x = 395 mm. Based on the results, displacements near the downstream edge focus on the following.

Figure 14 shows the contour maps of D_{rms} near the downstream edge, and (a) and (b) show D_{rms} calculated using all the fluctuations of D and only the fluctuating component of f_p, respectively. The abscissa and ordinate correspond to x

[DOI: 10.1299/jfst.2021jfst0005]

and z, respectively. The results suggest that D_{rms} increases at the spanwise edge of the downstream edge of the flag. However, it does not fluctuate at the frequency of f_p and the center of the downstream edge of the flag fluctuates at a higher frequency. The region is almost consistent with that enclosed in the white line shown in Fig. 11. Therefore, the region is considered as the main noise source of the flag because it rolls down and up with a frequency corresponding to f_p.

Figure 15 shows the results of frequency analysis of D measured at several streamwise locations at z =0. Similarly, Fig. 16 shows the results of frequency analysis of D measured at several spanwise locations at x = 395 mm. The sampling number and number of samples for averaging the frequency analysis of D are 3000 and 10, respectively. The abscissa and ordinate correspond to the frequency and D_{rms}, respectively, in both figures. The red, green, and blue lines in Fig. 15 show the results obtained at x = 395 mm, 380 mm, and 365 mm, respectively. Additionally, the red, green, blue, and black lines in Fig. 16 show the results obtained at z = 0, -35 mm, -70 mm, and -105 mm, respectively. The results suggest that a distinct peak is absent in the results, except for at f_p (60 Hz). The peak is most distinct at x = 395 mm, and becomes small and broad-banded at x = 365 mm. Additionally, it is also clearly observed at z = 0, -35 mm, and -70 mm. However, it was not observed at z = -105 mm. Therefore, the region in the range -70 mm < z < 70 mm near the downstream edge significantly flutters at frequency f_p.

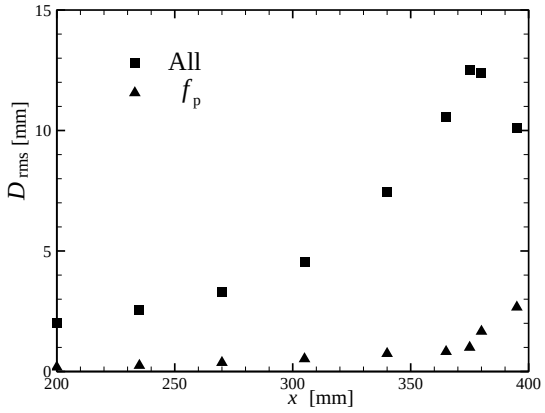

Fig. 13 Streamwise profiles of D_{rms}.

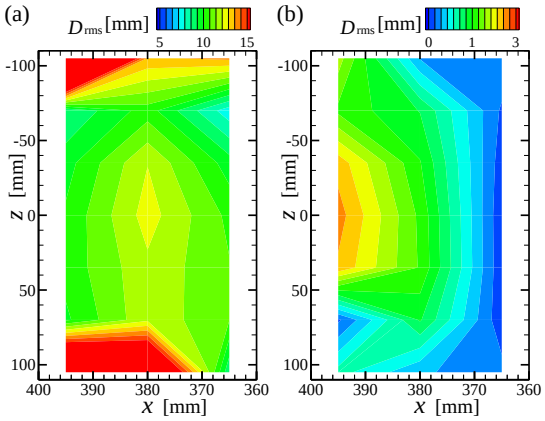

Fig. 14 Contour maps of D_{rms} calculated from (a) all fluctuations and (b) fluctuation of f_p.

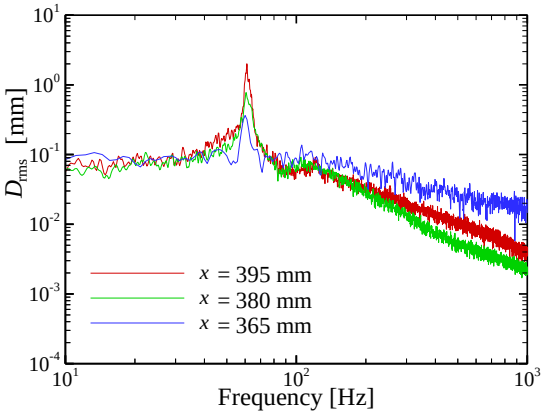

Fig. 15 Results of frequency analysis of D measured at x = 365, 380, and 395 mm (z = 0).

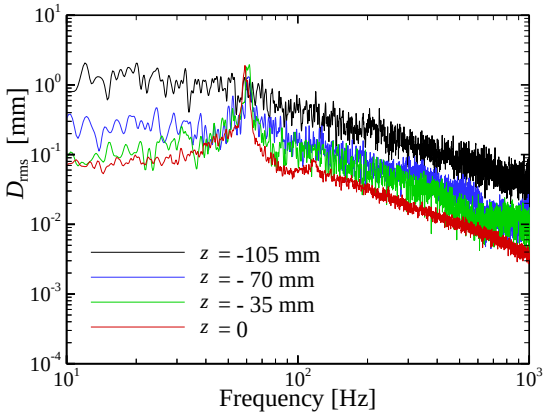

Fig. 16 Results of frequency analysis of D measured at z = 0, -35, -70, and -105 mm (x = 395 mm).

Figure 17 shows the cross-streamwise profiles of the cross-correlation coefficient of D and (a), (b), and (c) in Fig. 17 show the profiles corresponding to U_∞ = 30, 25, and 20 m/s, respectively. The abscissa and ordinate correspond to z and the cross-correlation coefficient, respectively. The red, green, and blue symbols in Fig. 17 correspond to the results obtained at x = 395 mm, 380 mm, and 365 mm, respectively. The reference signal used to calculate the cross-correlation coefficient corresponds to D at z = 0. Therefore, it corresponds to 1 at z = 0 in Fig. 17. The number of data points used

[DOI: 10.1299/jfst.2021jfst0005]

for the calculation of the cross-correlation is 30,000. The results indicate that the cross-correlation decreases at the downstream edge of the flag. This indicates that the two-dimensionality of the displacement of the flag decreases at the downstream edge. The results also indicate that it is relatively higher when U_∞ is slow (i.e., U_∞ = 20 m/s). Furthermore, the findings reveal that the cross-correlation coefficient at x = 395 mm when U_∞ is 30 m/s is lower than that when U_∞ is 25 m/s. Therefore, it is considered that the differences lead to the emission of sound pressure when U_∞ = 25 m/s exceeds that when U_∞ = 30 m/s, as shown in Fig. 9.

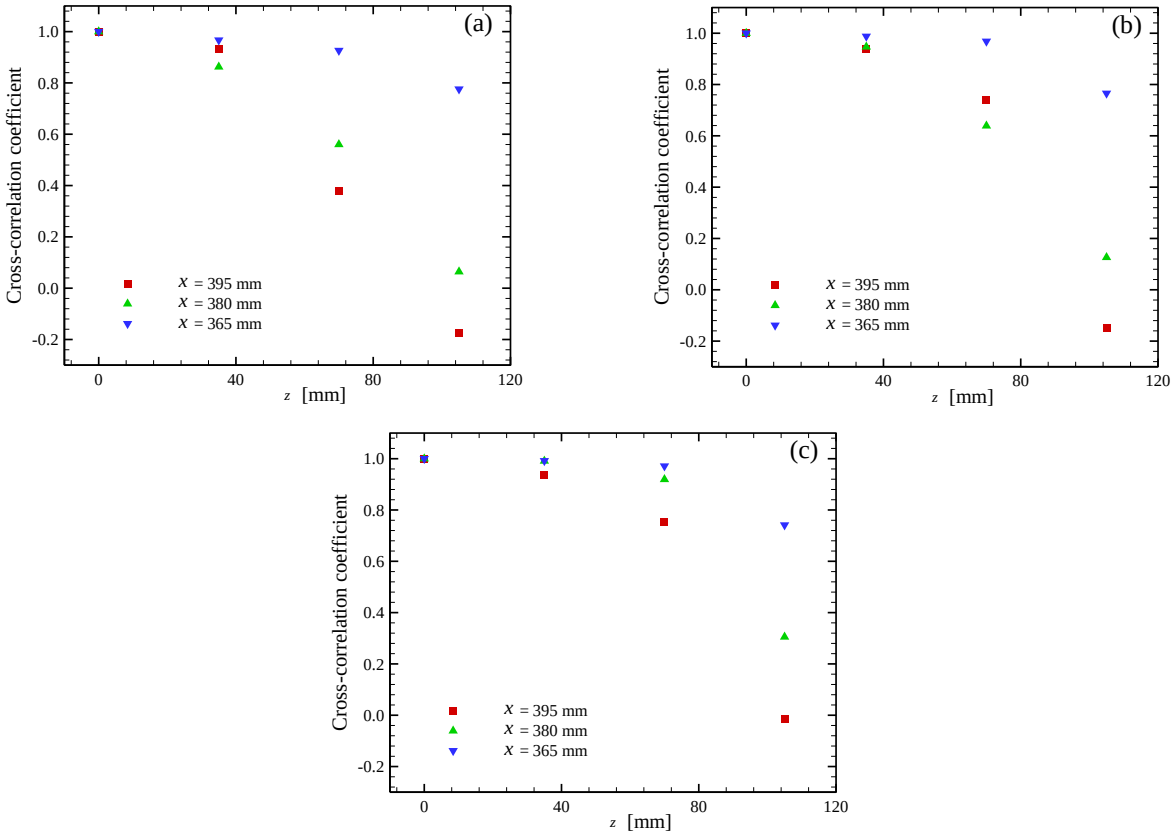

Fig. 17 Cross-streamwise profiles of the cross-correlation coefficient of D. (a) U_∞ = 30 m/s, (b) U_∞ = 25 m/s, and (c) U_∞ = 20 m/s.

3.4 Flow field near the downstream edge

PIV (Particle Image Velocimetry) was used to measure the mean and instantaneous velocity fields at the downstream of the flag. The camera (Photron Inc., FASTCAM SA-X2) was set at the lateral side of the flag, and seeding particles with a diameter of approximately 1 μm were introduced into the airflow. The particles were irradiated with a YAG laser to capture an instant image. The photographing section was set to z = 0. The flow velocity was calculated using the adaptive correlation algorithm (DANTEC Dynamic Studio, Adaptive PIV). The inspection area in the correlation analysis was 32 × 32 pixels, and the overlap was 50 %. The spatial resolution of the velocity vector is 6 mm, and the resulting velocity field is 345 mm in the x direction and 216 mm in the y direction. The sampling frequency used to obtain the instantaneous velocity field was 10 kHz. It should be noted here that the PIV measurements were performed in a closed-type small low-turbulence wind tunnel at the Institute of Fluid Science, Tohoku University.

Figures 18-20 show the contour maps of the instantaneous streamwise velocity U and cross-streamwise velocity V with velocity vectors at Time 1, 2, and 3, respectively. The inlet velocity at the nozzle exit U_∞ was 30 m/s. Fig. 18 shows the strong downward flow near the downstream edge of the flag when it is rolling down. Similarly, Fig. 20 indicates that the strong upward flow can be found near the edge when the flag is rolling up. Further, Fig. 19 shows that there is no strong upward or downward flow near the edge, and the direction of the flow is relatively straight when the downstream edge of the flag is flat.

The results shown in this chapter indicate that the strong upward or downward flow near the downstream edge of the

[DOI: 10.1299/jfst.2021jfst0005]

flag causes vibration and noise generation. These characteristic flows occur periodically, and their period depends on l, m, and U_∞ because they determine the flow field near the downstream edge. Furthermore, if these strong upward or downward flows occur at the same time for every spanwise location of the flag, the cross-correlation coefficient of D, which is shown in Fig. 17, becomes large and it generates loud noise.

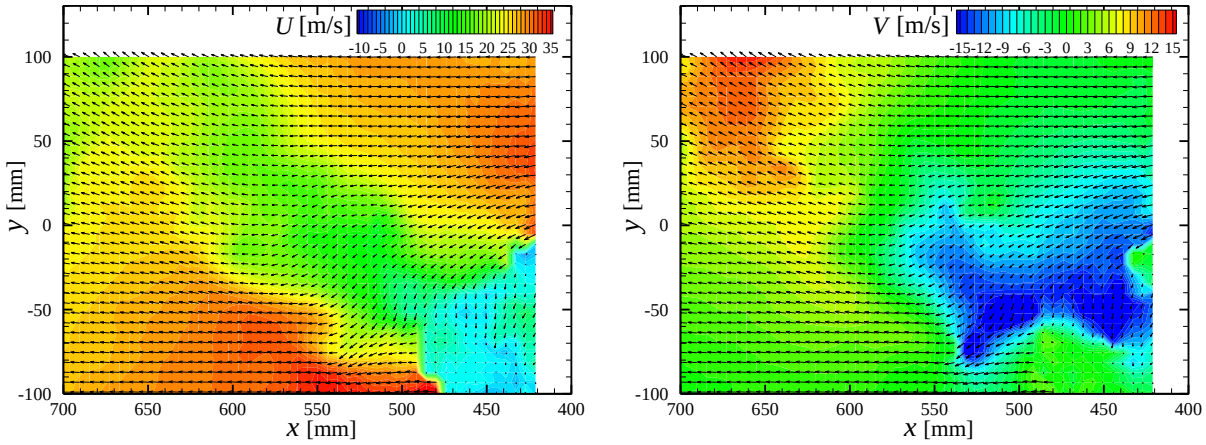

Fig. 18 Contour maps of U and V with velocity vectors at the downstream of the flag (Time 1, U_∞ = 30 m/s).

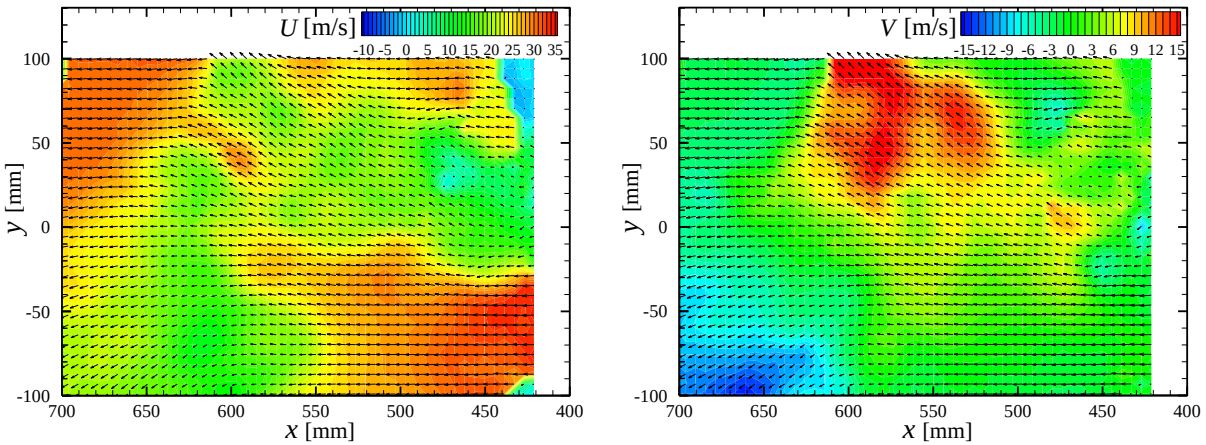

Fig. 19 Contour maps of U and V with velocity vectors at the downstream of the flag (Time 2, U_∞ = 30 m/s).

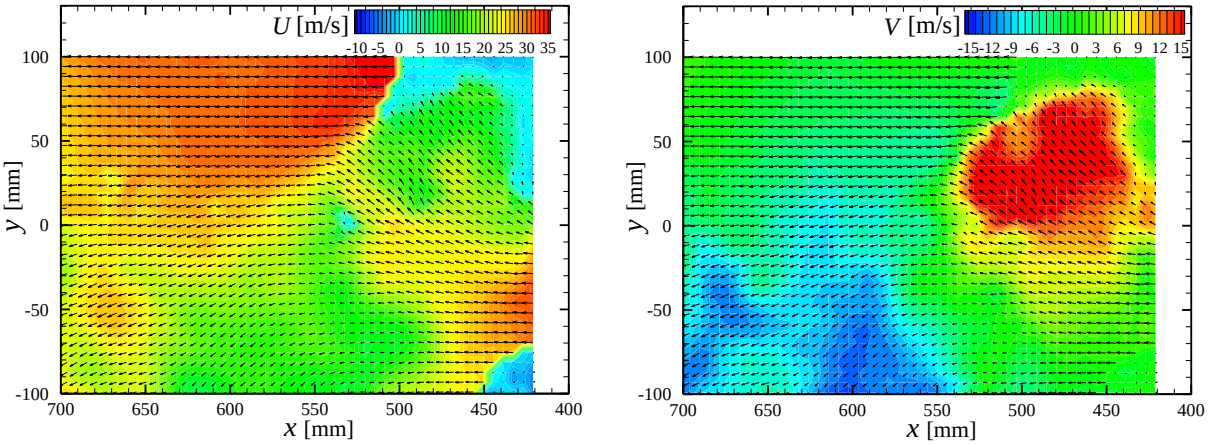

Fig. 20 Contour maps of U and V with velocity vectors at the downstream of the flag (Time 3, U_∞ = 30 m/s).

[DOI: 10.1299/jfst.2021jfst0005]

4. Conclusion

In this study, we performed experiments in a low-noise wind tunnel to investigate the characteristics and generation mechanism of noise from a flag. The results of the study are summarized as follows:

(1) A highly periodic noise with significant directivity in the vertical direction was generated from a fluttering flag.
(2) The dominant frequency of the noise f_p was linearly proportional to the velocity at the nozzle exit U_∞. Furthermore, it is inversely proportional to the length of the flag l and square root of the thickness of the flag $\sqrt{t}$.
(3) The downstream edge of the flag rolled up and down when a significant periodic sound pressure was generated.
(4) Near the center of the downstream edge, the flag fluttered at the dominant frequency of the noise f_p with high two-dimensionality. Therefore, the region was considered to be the source of the flag noise.
(5) A strong upward or downward flow near the downstream edge of the flag causes vibration and noise generation. These characteristics flow periodically, and their period depends on l, m, and U_∞ because they determine the flow field near the downstream edge of the flag.

Acknowledgements

Part of the work was carried out under the Collaborative Research Project of the Institute of Fluid Science, Tohoku University. This work was also partially supported by JSPS Kakenhi Grant Number 18K136911 and TEPCO Memorial Foundation.

Nomenclature

D	:	Displacement of the flag [mm]
D_{rms}	:	Root mean square value of the displacement [mm]
f_p	:	Peak frequency of the noise [Hz]
l	:	Length of the flag [mm]
MR	:	Mass ratio [-]
m	:	Mass of the flag [kg]
S_t	:	Normalized frequency [-]
t	:	Thickness of the flag [mm]
U_∞	:	Velocity at the nozzle exit [m/s]
U	:	Instantaneous streamwise velocity [m/s]
V	:	Instantaneous cross-streamwise velocity [m/s]
w	:	Width of the flag [mm]
x	:	Streamwise coordinate [mm]
y	:	Cross-streamwise coordinate [mm]
z	:	Spanwise coordinate [mm]
ρ	:	Density of fluid [kg/m^3]

References

Blake, W. K., Mechanics of flow-induced sound and vibration (2nd edition), Volume 1: General Concepts and Elementary Sources, Academic press (2017).

Carruthers, A. C. and Filippone, A., Aerodynamic drag of streamers and flags, Journal of Aircraft, Vol. 42, No. 4 (2005), pp. 976-982.

Chen, Y., Yu, Y., Zhou, W., Peng, D. and Liu, Y., Heat transfer enhancement of turbulent channel flow using tandem self-oscillating inverted flags, Physics of Fluids, Vol. 30 (2018), 075108.

Emmanuel, V., Xavier, A. and Pascal, H., Fluttering flags: An experimental study of fluid forces, Journal of Fluids and Structures, Vol. 43 (2013), pp. 385-401.

Farithorne, R. A., Drag of Flags, Aeronautical Research Committee, Reports and Memoranda, Vol. 1345 (1930), pp. 887-

[DOI: 10.1299/jfst.2021jfst0005]

891.
Hoerner, S. F., Fluid-Dynamic Drag, Published by the author, Vol. 25 (1965), Chapter 3.
Kim, D., Cosse, J., Cerdéira, C. H. and Gharib, M., Flapping dynamics of an inverting flag, Journal of Fluid Mechanics, Vol. 736 (2013).
Kim, S., Huang, W. X., Sung, H. J., Constructive and destructive interaction modes between two tandem flexible flags in viscous flow, Journal of Fluid Mechanics, Vol. 661 (2010), pp. 511-521.
Moretti, P. M., Tension in fluttering flags, International Journal of Acoustics and Vibration, Vol. 8, No. 4 (2003), 227-230.
Morris-Thomas, M. T. and Steen, S., Experiments on the stability and drag of a flexible sheet under in-plane tension in uniform flow, Journal of Fluids and Structures, Vol. 25 (2009), pp. 815-830.
Ristorph, L. and Zhang, J., Anomalous hydrodynamics drafting of interacting flapping flags, Physical Review Letters, Vol. 101 (2008), 194502.
Ryu, J., Park, S. G., Kim, B. and Sung, H. J., Flapping dynamics of an inverted flag in a uniform flow, Journal of Fluids and Structures, Vol. 57 (2015), pp. 159-169.
Sparenberg, J. A., On the waving motion of a flag, Proceedings of Koninklijke Nederlandse Akademie van Wetenschappen, Series B: Physical Sciences, Vol. 65 (1962).
Taneda, S., Waving motions of flags, Journal of the Physical Society of Japan, Vol. 24, No. 2 (1968), pp. 392-401.
Thoma, D., Warum flattert die Fahne?, Mitteilungen des Hydraulischen Institus der Technischen Hochschule Münschen, Vol. 9, pp. 30-34.
Yu, Y., Liu, Y. and Chen, Y., Vortex dynamics behind a self-oscillating inverted flag placed in a channel flow: Time-resolved particle image velocimetry measurements, Physics of Fluids, Vol. 20 (2017), 125104.

[DOI: 10.1299/jfst.2021jfst0005]